Preprint
2016; **00**:1–15

Optimal control for reinitialization in finite element level set methods

Christopher Basting[1,*], Dmitri Kuzmin[1] and John N. Shadid[2,3]

[1] *Institute of Applied Mathematics (LS III), TU Dortmund University, Vogelpothsweg 87, D-44227 Dortmund, Germany*
[2] *Computational Mathematics Dept., Sandia National Laboratories, P.O. Box 5800, Albuquerque, NM 87185, USA*
[3] *Department of Mathematics and Statistics, University of New Mexico, MSC01 1115, Albuquerque, NM 87131, USA*

SUMMARY

A new optimal control control problem that incorporates the residual of the Eikonal equation into its objective is presented. The formulation of the state equation is based on the level set transport equation but extended by an additional source term, correcting the solution so as to minimize the objective functional. The method enforces the constraint so that the interface cannot be displaced. The system of first order optimality conditions is derived, linearized, and solved numerically. The control also prevents numerical instabilities, so that no additional stabilization techniques are required. This approach offers the flexibility to include other desired design criteria into the objective functional. The approach is evaluated numerically in three different examples and compared to other PDE-based reinitialization techniques.

Received ...

KEY WORDS: Level set evolution; Reinitialization; Optimal Control; Variational formulation; Finite element methods; Eikonal equation

1. INTRODUCTION

Level set methods are among the most popular techniques for numerical simulation of evolving interfaces in the context of interface capturing methods. The interface is represented in an implicit manner as the zero level set of an auxiliary function, the level set function. When applied to free-surface problems, the smoothness of this function at the interface is of great importance. Signed distance functions generally satisfy this need and are therefore commonly chosen as initial data. Unfortunately, the desirable signed distance function property is not preserved in the numerical process of advection. In some regions the level set function can become very steep, so that a nearly discontinuous function has to be advected. In other regions it may become very flat causing a significant loss of accuracy when localizing the interface. In order to preserve the signed distance function property approximately, reinitialization procedures are commonly applied. Those are roughly divided into geometric and PDE-based procedures. A wealth of geometric [1, 2, 3] and PDE-based techniques [4, 5, 6, 7, 8, 9] exist.

A well designed reinitialization method produces an approximation to a signed distance function that has the same zero isocontour as the original level set function. Sussman et al. [7] presented a post processing reinitialization scheme in which a hyperbolic PDE is solved to steady state. In practice, the numerical solution of this equation leads to significant displacements of the interface [10] due to artificial diffusion. An approach directly addressing this inaccuracy is the interface local projection method of Parolini [6]. Here, in a narrow band along the interface, the values of the

*Correspondence to: Christopher Basting (christopher.basting@math.tu-dortmund.de)

level set function are directly computed and then used to provide boundary conditions for a post-processing reinitialization scheme.

As alternative approach to hyperbolic reinitialization, Li et al. [5] introduce the distance regularized level evolution (DRLSE). Its corrected level set function is the steady-state solution to an energy-minimizing gradient flow equation. The approach offers the flexibility to choose a potential function defining the distance regularization, so that truncated distance functions can also be handled, but special care needs to be taken to prevent interface displacements. In our recent publication [11], we built on this idea and developed an interface preserving level set reinitialization scheme, leading to a nonlinear elliptic problem that penalizes interface displacements. In the present paper we will comment on this approach combined with the interface local projection method by Parolini [6].

In the context of moving interfaces, all of the approaches mentioned above are correcting a given predictor to the solution of the advection equation. In contrast to this procedure, Ville et al. [9] propose an all-at-once approach that embeds the reinitialization equation of [7] into the transport equation. The method is referred to as convective reinitialization. Here, interface accuracy relies on how well the sign function is resolved.

In this paper we present another all-at-once approach based on an optimal control problem. The residual of the Eikonal equation is minimized whilst constraining an augmented transport equation. We derive the resulting nonlinear system of first order optimality conditions and linearize it. Three numerical examples illustrate the potential of this new approach.

2. LEVEL SET METHOD

The level set approach to simulating the evolution of a free interface Γ inside a bounded domain Ω is based on an implicit representation of Γ in terms of a scalar indicator function $\varphi(t, \mathbf{x})$ such that

$$\Gamma(\varphi)(t) = \{\mathbf{x} \in \Omega \mid \varphi(t, \mathbf{x}) = 0\}. \tag{1}$$

In the context of two-phase flows, the sign of φ tells the two phases apart. It is common practice to initialize φ as signed distance function to the zero level set, i.e.

$$\varphi(0, \mathbf{x}) = \pm\mathrm{dist}(\mathbf{x}, \Gamma(0)). \tag{2}$$

A signed distance function satisfies the Eikonal equation

$$|\nabla\varphi| = 1, \tag{3}$$

almost everywhere. If φ is a signed distance function (SDF), the normal vector to the interface is readily obtained by

$$\mathbf{n} = \nabla\varphi. \tag{4}$$

This is particularly useful when it comes to recovering interface related quantities such as the curvature. The signed distance function property is also very useful in the context of adaptive strategies, since it serves as interface proximity indicator. Furthermore, when numerically solving the level set transport equation

$$\frac{\partial\varphi}{\partial t} + \mathbf{v} \cdot \nabla\varphi = 0 \qquad \text{in } \Omega, \tag{5}$$

reinitialization of φ will ensure $|\nabla\varphi| \approx 1$, thus preventing numerical instabilities due to steepening and flattening effects as described above. Numerical methods generally fail to preserve this desirable SDF property over time, wherefore reinitialization methods are commonly applied.

3. REINITIALIZATION

A well-designed reinitilization scheme should possess three important properties. Most importantly, the boundary condition $\varphi|_\Gamma = 0$ should be satisfied as closely as possible, i.e. the zero isocontour of φ must not be displaced in any significant manner by the reinitialization procedure. Second, the result should satisfy the SDF property and be smooth away from kinks. In particular, the residual of $|\nabla\varphi| = 1$ should be small in proximity to the interface where accuracy is most important. Last but not least, computational efforts due to reinitialization must be managable.

Many algorithms to tackle the problem of reinitialization exist and can roughly be subdivided into direct and PDE-based methods. Latter ones do not require the explicit localization of the interface but an approximate distance function is obtained by solving an additional or modified PDE. In this paper we focus on reinitialization methods mainly designed for evolution problems, i.e. methods of particular interest are those that approximate the solution to the interface transport equation while enforcing the SDF property in a certain way, which we will refer to as all-at-once methods. The alternative are post-processing approaches, where the numerical solution to the transport equation $\tilde{\varphi}$ serves as a predictor and the reinitialization method then corrects $\tilde{\varphi}$ to become a good approximation to a signed distance function.

3.1. Hyperbolic Reinitialization

The most common PDE-based approach was introduced by Sussman et al. [7]. Due to the methods hyperbolic nature, we refer to this approach as hyperbolic reinitialization. The key idea boils down to solving the initial value problem

$$\frac{\partial\varphi}{\partial\tau} + S_\varepsilon(\tilde{\varphi})(|\nabla\varphi| - 1) = 0, \qquad \varphi(0,\mathbf{x}) = \tilde{\varphi}, \tag{6}$$

in virtual time τ to steady state. S_ε is a regularization of the sign function; a commonly chosen one is

$$S_\varepsilon(\tilde{\varphi}) = \frac{\tilde{\varphi}}{\sqrt{\tilde{\varphi}^2 + \varepsilon^2}}.$$

Since $S_\varepsilon(\tilde{\varphi})$ vanishes where $\varphi = 0$, the steady state solution to (6) preserves the implicitly defined interface $\Gamma(\tilde{\varphi})$ exactly. Furthermore, the steady state φ satisfies the Eikonal equation $|\nabla\varphi| = 1$ almost everywhere. As already pointed out, this method avoids the explicit localization of the interface. However, numerically this approach requires a well-chosen and mesh-size dependent regularization parameter ε (its choice is not clear) and a stable scheme to solve the equation to steady state. Inappropriate choices of ε may lead to slow speed of convergence and considerable displacements of the interface due to the added numerical diffusion. This may affect the global mass conservation properties of the overall scheme significantly, see for example [12].

Convected Reinitialization

Based on the hyperbolic reinitializaton approach, Ville et al. [9] embed the reinitialization process into the actual transport model, transforming the post-processing into an all-at-once method. The convected reinitialization equation

$$\frac{\partial\varphi}{\partial t} + \mathbf{v}\cdot\nabla\varphi + \lambda S(\varphi)(|\nabla\varphi| - 1) = 0, \tag{7}$$

is obtained by considering the auxillary intial value problem (6) in virtual time τ, chosing the parameter

$$\lambda = \frac{\partial\tau}{\partial t}, \tag{8}$$

and rewriting it into an Eulerian context. At the interface, $S(\tilde{\varphi})$ is zero and the source term vanishes. The numerical solution of (7) however requires a regularized signed distance function introducing an additional parameter as well as an iterative scheme to linearize the problem.

In terms of a finite element discretization, Ville et al. [9] suggest an streamline-upwind Petrov-Galerkin (SUPG) method to solve this convection dominated problem with coefficient

$$\tau_{\mathsf{SUPG}} \simeq \frac{h}{D|\mathbf{v}|}, \tag{9}$$

where D is the number of nodes per element and h is the mesh size. The problem can easily be linearized by means of a fixed-point iteration or Newton's method. Usually a couple of virtual time steps are sufficient. The scheme is sensitive to the choice of λ and may require smaller choices of λ than (8) which may increase the number of artificial time steps required.

3.2. *Parabolic Reinitialization*

A different approach to hyperbolic PDE reinitialization is the DRLSE algorithm developed by Li et al. [5]. In the context of pure reinitialization, the corrected level set function represents the steady-state solution to an energy-minimizing gradient flow equation

$$\frac{\partial \varphi}{\partial \tau} + \frac{\partial \mathcal{R}}{\partial \varphi} = 0, \tag{10}$$

where $\mathcal{R}(\varphi)$ is a suitable energy functional [11]. The choice

$$\mathcal{R}(\varphi) = \frac{1}{2}\int_\Omega (|\nabla \varphi| - 1)^2 \mathrm{d}x \tag{11}$$

is the least-squares solution to (3). For this particular choice, (10) reduces to the nonlinear heat equation

$$\frac{\partial \varphi}{\partial \tau} - \nabla \cdot \left(\nabla \varphi - \frac{\nabla \varphi}{|\nabla \varphi|} \right) = 0. \tag{12}$$

The initial condition for the steady-state computations is given by the original level set function $\tilde{\varphi}$. For other definitions of the energy functional $\mathcal{R}(\varphi)$, see [5, 11].

3.3. *Elliptic Reinitialization*

In [11] the authors presented a different approach based on the presented parabolic reinitialization but yielding an elliptic problem instead. In contrast to the local hyperpolic reinitialization approach needed to be carried out to steady state, the elliptic approach is global and hence produces a solution in just one step – justifying the higher computational costs. However, since the problem is nonlinear, a fixed-point iteration needs to be applied. In practice, only one or very few iterations are needed for it to produce sufficiently good results.
The method is based on a general energy functional (see also [5])

$$\mathcal{R}_p(\varphi) = \frac{1}{2}\int_\Omega p(|\nabla \varphi|) \mathrm{d}x, \tag{13}$$

depending on a suitably chosen potential function $p : [0, \infty) \to \mathbb{R}$. For

$$p(s) := (s-1)^2 \tag{14}$$

we obtain the particular choice of (11). To enforce the boundary condition $\varphi|_{\Gamma(\tilde{\varphi})} = 0$ imposed by the original level set function $\tilde{\varphi}$, the cost functional is augmented by adding the penalty term

$$\mathcal{P}_{\tilde{\varphi}}(\varphi) = \frac{\alpha}{2}\int_{\Gamma(\tilde{\varphi})} \varphi^2 \mathrm{d}s, \tag{15}$$

where $\tilde{\varphi}$ denotes the provisional solution before applying the reinitialization scheme. The penalized minimization problem yields the necessary optimality conditions

$$\frac{\partial \mathcal{R}_p}{\partial \varphi} + \frac{\partial \mathcal{P}_{\tilde{\varphi}}}{\partial \varphi} = 0. \tag{16}$$

The variational form of the penalized minimization process becomes

$$\int_\Omega d_p(|\nabla \varphi|) \nabla \varphi \cdot \nabla v \mathrm{d}x + \alpha \int_{\Gamma(\tilde{\varphi})} \varphi v \mathrm{d}s, \tag{17}$$

with diffusion rate $d_p(s) = \frac{p'(s)}{s}$. This representation reveals that the level set regularization term generates forward diffusion for $d_p(|\nabla\varphi|) > 0$ and backward diffusion for $d_p(|\nabla\varphi|) < 0$, respectively.
The variational problem can be solved using a Ritz-Galerkin finite element method. The variational form associated with (16) and for the particular choice (14) is given by

$$\int_\Omega \left(1 - \frac{1}{|\nabla\varphi|}\right) \nabla\varphi \cdot \nabla v \mathrm{d}x + \alpha \int_{\Gamma(\tilde{\varphi})} \varphi v \mathrm{d}s, \tag{18}$$

and can be linearized into a consistent fixed-point iteration where at each step a steady diffusion-reaction equation with a source term depending on the gradient of the previous iterate has to be solved.
Note that other choices of p lead to different diffusion rates and can, for example, preserve flat gradients of φ away from the interface; see [11] for more details.

Local Projection Penalty Term
The method presented in [11] can be modified as follows: instead of enforcing the boundary condition $\varphi|_{\Gamma(\tilde{\varphi})} = 0$ by adding a surface penalty term such as (15), deviations from a desired state are penalized. This desired state is defined by the local L^2 projection of an exact but discontinuous reinitialization of $\tilde{\varphi}$ in the interface proximity region Ω_{int}. This local projection technique was developed by Parolini [6]. Applied to elliptic reinitialization, the energy functional $\mathcal{R}$ and the penalty

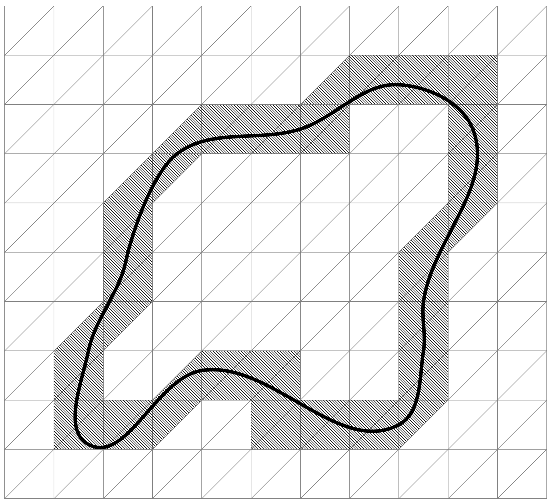

Figure 1. Interface region Ω_{int} (shaded)

term $\mathcal{P}$ change to

$$\mathcal{R}(\varphi) = \frac{1}{2} \int_{\Omega\setminus\Omega_{\text{int}}} p(|\nabla\varphi|)\mathrm{d}x, \tag{19}$$

and

$$\mathcal{P}(\varphi) = \alpha \int_{\Omega_{\text{int}}} (\varphi - \varphi_{\text{int}})^2 \mathrm{d}x, \tag{20}$$

with the local L^2 projection

$$\int_{\Omega_{\text{int}}} \varphi_{\text{int}} v \mathrm{d}x = \int_{\Omega_{\text{int}}} \frac{\tilde{\varphi}}{|\nabla\tilde{\varphi}|} v \mathrm{d}x. \tag{21}$$

Note that the $\frac{\tilde{\varphi}}{|\nabla\tilde{\varphi}|}$ satisfies the Eikonal equation and its zero level set coincides with $\tilde{\varphi}$. Both approaches yield very similar results; however the local projection is easier to implement as no explicit localization of the interface is required.

4. OPTIMAL CONTROL APPROACH

We now present an optimal control approach designed as all-at-once method, i. e. solving the level set transport equation while constraining the Eikonal residual. In this method the transport equation is augmented by a source term φu and serves as a constraint for the optimization problem. The objective functional consists of the energy functional $\mathcal{R}_p(\varphi)$ as introduced in (13) and a Tikonov regularization term for the control variable u. The optimization problem is formulated as follows:

$$\min J(\varphi, u) := \frac{1}{2}\mathcal{R}_p(\varphi) + \frac{\beta}{2}\|u\|_U^2\,, \tag{22a}$$

$$\text{subject to} \quad \frac{\partial \varphi}{\partial t} + \mathbf{v}\cdot\nabla\varphi + \varphi u = 0. \tag{22b}$$

A suitable control space has to be chosen, for example $U = L^2(\Omega)$. Since the added source term vanishes where $\varphi = 0$, the zero isocontour is not displaced by definition of the method even though no further regularization (e. g. of the sign function as in [7, 9]) is required. Elsewhere, the control adjusts the added source term so that the residual of the Eikonal equation is minimized under the given objective. The choice of U and β determine the expected regularity of the control.

4.1. Weak Form

The state equation (22b) can be written in weak form as

$$\int_\Omega \left(\frac{\partial \varphi}{\partial t} + \mathbf{v}\cdot\nabla\varphi + \varphi u\right) v \,\mathrm{d}x,$$

defining a bilinear form $\mathsf{a}(\cdot,\cdot)$ and a trilinear form $\mathsf{b}(\cdot,\cdot,\cdot)$. We will consider different schemes for discretization and stabilization, each resulting in specific linear forms. For simplicity we restrict ourselves to the time-discrete problem. Let φ^n denote the solution of the previous time level t^n. The added source term is treated fully implicitly. The semi-discrete problem then reads

$$\min J(\varphi, u) := \mathcal{R}_p(\varphi) + \frac{\beta}{2}\|u\|_U^2\,, \tag{23a}$$

$$\text{subject to} \quad \mathsf{a}(\varphi, v) + \mathsf{b}(\varphi, u, v) = \mathsf{l}(v) \qquad \forall v. \tag{23b}$$

Since the state equation is convection dominated, stabilized numerical schemes are preferred but not necessarily required in the optimal control approach where the control will stabilize the solution. We will consider the following three approaches:

1. θ-scheme and no stabilization

$$\mathsf{a}^{\mathsf{NS}}(\varphi, v) = \int_\Omega \varphi v + \Delta t\theta\mathbf{v}\cdot\nabla\varphi v \mathrm{d}x, \tag{24a}$$

$$\mathsf{b}^{\mathsf{NS}}(\varphi, u, v) = \int_\Omega \Delta t\varphi u v \mathrm{d}x, \tag{24b}$$

$$\mathsf{l}^{\mathsf{NS}}(v) = \int_\Omega \varphi^n v - \Delta t(1-\theta)\mathbf{v}\cdot\nabla\varphi^n. \tag{24c}$$

2. θ-scheme and SUPG stabilization (with parameter τ)

$$\mathsf{a}^{\mathsf{SUPG}}(\varphi, v) = \int_\Omega \big(\varphi + \Delta t\theta\mathbf{v}\cdot\nabla\varphi\big)(v + \tau\mathbf{v}\cdot\nabla v)\mathrm{d}x, \tag{25a}$$

$$\mathsf{b}^{\mathsf{SUPG}}(\varphi, u, v) = \int_\Omega \Delta t\varphi u(v + \tau\mathbf{v}\cdot\nabla v)\mathrm{d}x, \tag{25b}$$

$$\mathsf{l}^{\mathsf{SUPG}}(v) = \int_\Omega \big(\varphi^n - \Delta t(1-\theta)\mathbf{v}\cdot\nabla\varphi^n\big)(v + \tau\mathbf{v}\cdot\nabla v)\mathrm{d}x. \tag{25c}$$

3. Semi-Implicit Lax-Wendroff (SILW) stabilization

$$\mathsf{a}^{\mathsf{SILW}}(\varphi, v) = \int_\Omega \varphi v + \frac{(\Delta t)^2}{2}(\mathbf{v}\cdot\nabla\varphi)(\mathbf{v}\cdot\nabla v)\mathrm{d}x, \tag{26a}$$

$$\mathsf{b}^{\mathsf{SILW}}(\varphi, u, v) = \int_\Omega \Delta t\varphi u v \mathrm{d}x, \tag{26b}$$

$$\mathsf{l}^{\mathsf{SILW}}(v) = \int_\Omega -\Delta t\mathbf{v}\cdot\nabla\varphi^n v. \tag{26c}$$

4.2. Optimality Conditions

We derive the first order optimality conditions for (23) by differentiating the associated Lagrangian functional

$$\mathcal{L}(\varphi, u, \lambda) := J(\varphi, u) + \mathsf{a}(\varphi, \lambda) + \mathsf{b}(\varphi, u, \lambda) - \mathsf{l}(\lambda) \tag{27}$$

with respect to state φ, control u and Lagrange multiplier λ:

$$\delta\mathcal{R}(\varphi, \psi) + \mathsf{a}(\psi, \lambda) + \mathsf{b}(\psi, u, \lambda) - \mathsf{l}(\lambda) = 0 \qquad \forall\psi \tag{28a}$$

$$\mathsf{b}(\varphi, \eta, \lambda) + \beta(u, \eta)_U = 0 \qquad \forall\eta \tag{28b}$$

$$\mathsf{a}(\varphi, v) + \mathsf{b}(\varphi, u, v) = \mathsf{l}(v) \qquad \forall v \tag{28c}$$

The derivative of $\mathcal{R}_p(\varphi)$ with respect to φ in direction v is given by

$$\delta\mathcal{R}_p(\varphi, v) = \int_\Omega p'(|\nabla\varphi|)\frac{\nabla\varphi\cdot\nabla v}{|\nabla\varphi|}\mathrm{d}x, \tag{29}$$

and similarly, the second derivative is

$$\begin{aligned}\delta^2\mathcal{R}_p(\varphi, v, w) &= \int_\Omega p''(|\nabla\varphi|)\frac{\nabla\varphi\cdot\nabla w}{|\nabla\varphi|}\frac{\nabla\varphi\cdot\nabla v}{|\nabla\varphi|}\mathrm{d}x \\ &\quad + \int_\Omega p'(|\nabla\varphi|)\left(\frac{\nabla w\cdot\nabla v}{|\nabla\varphi|} - \frac{\nabla\varphi\cdot\nabla v}{|\nabla\varphi|^2}\frac{\nabla w\cdot\nabla\varphi}{|\nabla\varphi|}\right)\mathrm{d}x \\ &= \int_\Omega \frac{p''(|\nabla\varphi|)}{|\nabla\varphi|^2}\nabla\varphi\cdot\nabla w\nabla\varphi\cdot\nabla v\mathrm{d}x \\ &\quad + \int_\Omega \frac{p'(|\nabla\varphi|)}{|\nabla\varphi|}\left(\nabla w\cdot\nabla v - \frac{(\nabla\varphi\cdot\nabla v)(\nabla\varphi\cdot\nabla w)}{|\nabla\varphi|^2}\right)\mathrm{d}x\end{aligned}$$

For p_1, we have $p_1'(s) = s - 1$, $p_1''(s) = 1$, whence

$$\delta\mathcal{R}_1(\varphi, v) = \int_\Omega \left(1 - \frac{1}{|\nabla\varphi|}\right)\nabla\varphi\cdot\nabla v\mathrm{d}x,$$

and

$$\delta^2\mathcal{R}_2(\varphi, v, w) = \int_\omega \nabla v\cdot\nabla w\left(1 - \frac{1}{|\nabla\varphi|}\right) + \frac{(\nabla\varphi\cdot\nabla v)(\nabla\varphi\cdot\nabla w)}{|\nabla\varphi|^3}\mathrm{d}x.$$

4.3. Linearization

To solve system (28) numerically, a linearization is required. For a potential function p chosen as in (14), the system can be linearized by employing an iterative solution strategy such as

$$\delta\mathcal{R}_1(\varphi, v) \approx \int_\Omega \nabla\varphi^m\cdot\nabla v\mathrm{d}x - \int_\Omega \frac{\nabla\varphi^{m-1}\cdot\nabla v}{|\nabla\varphi^{m-1}|}\mathrm{d}x.$$

and

$$\mathsf{b}(\varphi, u, \lambda) \approx \mathsf{b}(\varphi^{m-1}, u^m, \lambda^m).$$

Alternatively, we can employ Newton's method for linearization. Therefore, let us denote the residual of (28) by $F(\mathbf{x})$ where $\mathbf{x} := (\varphi, u, \lambda)$. The Newton update to solve (28) then reads

$$x^{m+1} = x^m - \big(J(x^m)\big)^{-1} F(x^m), \tag{30}$$

with the Jacobian

$$\big(J(x^m)\big)_{i,j} = \left(\frac{\partial F_i}{\partial x_j}\right). \tag{31}$$

The derivatives of F are:

$$\frac{\partial F_1}{\partial \varphi} = \delta^2 \mathcal{R}_p(\varphi, \delta\varphi, \psi), \tag{32a}$$
$$\frac{\partial F_1}{\partial u} = \mathsf{b}(\psi, \delta u, \lambda), \tag{32b}$$
$$\frac{\partial F_1}{\partial \lambda} = \mathsf{a}(\psi, \delta\lambda) + \mathsf{b}(\psi, u, \delta\lambda), \tag{32c}$$
$$\frac{\partial F_2}{\partial \varphi} = \mathsf{b}(\delta\varphi, \eta, \lambda), \tag{32d}$$
$$\frac{\partial F_2}{\partial u} = (\delta u, \eta)_U, \tag{32e}$$
$$\frac{\partial F_2}{\partial \lambda} = \mathsf{b}(\varphi, \eta, \delta\lambda), \tag{32f}$$
$$\frac{\partial F_3}{\partial \varphi} = \mathsf{a}(\delta\varphi, v) + \mathsf{b}(\delta\varphi, u, v), \tag{32g}$$
$$\frac{\partial F_3}{\partial u} = \mathsf{b}(\varphi, \delta u, v), \tag{32h}$$
$$\frac{\partial F_3}{\partial \lambda} = 0. \tag{32i}$$

Considering the fully discrete numerical scheme, the Jacobian matrix has the block structure

$$J = \begin{bmatrix} \delta^2 \mathcal{R}(\varphi) & \Delta t M(\lambda) & A + \Delta t M(u) \\ \Delta t M(\lambda) & \beta M & \Delta t M(\varphi) \\ \hat{A} + \Delta t M(u) & \Delta t M(\varphi) & 0 \end{bmatrix},$$

where A is the discretization matrix of the transport equation defined by the bilinear form $\mathsf{a}(\cdot,\cdot)$, and $M(\cdot)$ the weighted mass matrix corresponding to the trilinear form $\mathsf{b}(\cdot,\cdot,\cdot)$. Thus, the discretization and stabilization schemes differ only in the discretization matrices A and $M(\cdot)$.

4.4. *Influence of the Regularization Parameter β*

In this section we will assess the influence of the regularization parameter β for an examplary test case. Figure 2 shows the $L^2(\Omega)$ error, the $H^1(\Omega)$ error, the displacement error (33) and the residual of the Eikonal equation after one full revolution of the distance function of a circle on a circular mesh. Note that in the optimal-control context $\varphi \in H^1(\Omega)$ by definition of the objective functional. Each of the three discretizations described in the previous section produces very similar results. Therefore we restrict ourselves to the θ-method with no stabilization (24). Other test cases exhibit very similar error behavior for the choice of β.
In our numerical studies we observed that very small values of β will, as expected, admit larger controls leading to larger errors than using larger values of β. We found the choice of β between 10^{-3} and 10^{-1} to produce good results in all cases. No significant time dependence was observed in the below numerical experiments.

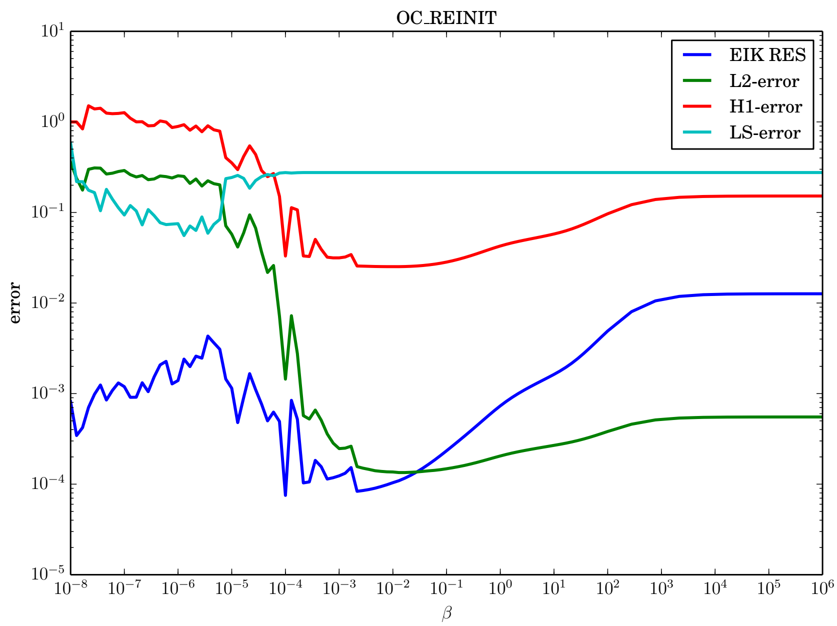

Figure 2. Influence of regularization parameter β on the errors of φ_h.

5. NUMERICAL RESULTS

To evaluate the error in terms of the displacement of the interface, we define

$$e_\Gamma = \frac{1}{N_\Gamma} \sum_{i \in P(\Gamma)} |D(\mathbf{x}_i) - \varphi_i|. \tag{33}$$

$P(\Gamma)$ denotes the set of nodes belonging to an element that is intersected by the zero isocontour, N_Γ is the number of such elements. To measure the overall quality of the signed distance function approximation, we evaluate the residual of the Eikonal equation in the L^2 sense and relative to the initial data:

$$e_E = \frac{\| |\nabla \varphi_h(t = T)| - 1 \|_{L^2(\Omega)}}{\| |\nabla \varphi_h(t = 0)| - 1 \|_{L^2(\Omega)}} \tag{34}$$

Other errors measured are the $L^2(\Omega)$ and $H^1(\Omega)$ error, given the finite element projection of the exact solution at the final time $t = T$. Note that the $H^1(\Omega)$ error will only provide information on the smoothness behavior, since we can only expect the optimal control solution to belong to $H^1(\Omega)$. For all results presented in the following, we used a second-order accurate time discretization (Crank-Nicolson or Semi-Implicit Lax-Wendroff) and linear finite elements for spatial discretization.

5.1. Mass Conservation

As already pointed out, reinitialization procedures may have an negative inlfuence on the local (and global) mass conservation as they can shift the interface. In the context of two-phase flows, knowledge of the exact interface location is crucial as it defines the mass contained within the interface. Errors in the interface position and thereby in conservation of mass significantly reduce numerical accuracy and may lead to unphysical behavior.
Therefore, in this first example we assess the quality of the reinitialization methods in terms of mass conservation. We consider two initial contours: a single circular interface, and a non-convex interface of two overlapping circles, each depicted in figure 3. The level set function is initialized as twice the signed distance function of the particular interface. Figures 4 and 5 show the initial

condition and its reinitialized counterpart. In tables I and II the corresponding numerical relative mass (area) errors

$$E = \frac{A(\varphi_h) - A_{\text{exact}}}{A_{\text{exact}}},$$

and rates of convergence are shown. Numerical computations were performed using linear finite elements on a uniform square mesh with mesh sizes $h_i = \frac{1}{20} \cdot \frac{1}{2^i}$, $i = 0, 1, 2, 3, 4$. Iterations were stopped when the residual of the Eikonal equation reached a value less than 1.1 times the Eikonal residual of the projected solution.

The L^2-projection of the initial data into the linear finite element space is second order accurate in terms of mass conservation. As pointed out in [6], the classical hyperbolic reinitialization approach (6) shows a convergence rate of ≈ 1. In contrast, both elliptic approaches and the optimal control approach exhibits a rate of ≈ 2 which is of the same order as direct brute-force reinitialization.

We want to emphasize the global character of the elliptic reinitialization: the results shown were obtained after only one iteration, which justifies the higher computational costs. Hyperbolic approaches need many iterations to reach steady state when provided a poor initial condition as in this test case. Furthermore, this example shows that the methods are not only capable of correcting a level set function that is close to a signed distance function but also generating a signed distance function from a given profile.

Due to the static nature of this test case, the optimal control approach is applied by setting the velocity field equal to zero. The observed larger absolute mass error can be justified by the design as an all-at-once method, where corrections are typically small within each time step whereas in this example large correction and hence large controls are needed. Clearly, large values of u will degrade the interface accuracy due to increased numerical diffusion in the source term. We also note that the other all-at-once method presented in the previous chapter, convective reinitialization, did not converge at all when applied to this test case.

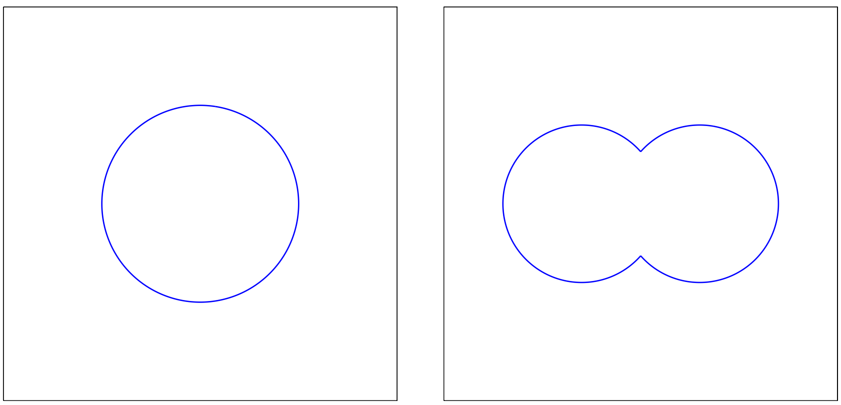

Figure 3. Test case interface shapes

h	Initial L^2 proj.		Elliptic reinit.		Elliptic reinit. w. L.P.		OC	
	Error	Order	Error	Order	Error	Order	Error	Order
0.050000	0.008928	2.2446	0.001486	-0.2100	0.006966	1.8986	0.046514	3.3584
0.025000	0.001884	2.1359	0.001719	2.0291	0.001868	2.1253	0.004535	1.9897
0.012500	0.000429	2.0632	0.000421	2.0294	0.000428	1.9757	0.001142	1.9831
0.006250	0.000103	2.0783	0.000103	1.9717	0.000109	1.9886	0.000289	1.8825
0.003125	0.000024		0.000026		0.000027		0.000078	

Table I. Convergence test: relative mass (area) error for the circular interface.

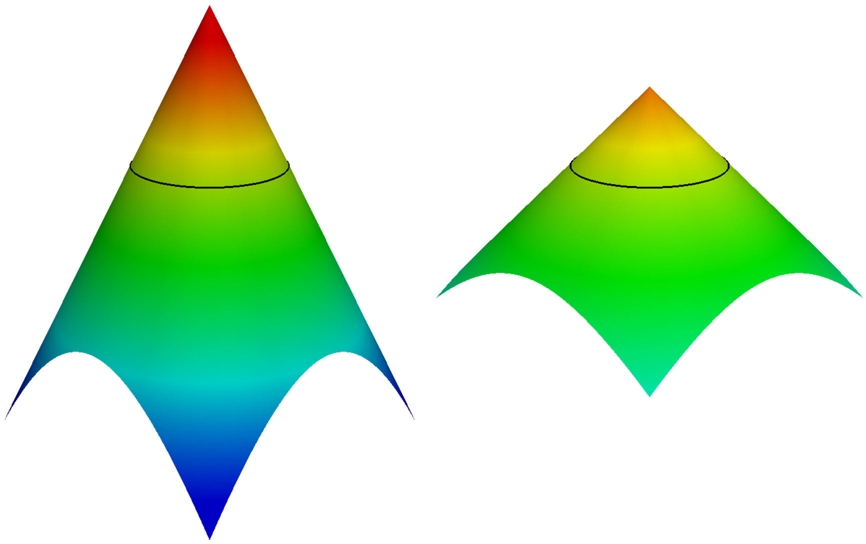

Figure 4. Circular interface: initial condition (left) and the level set function after reinitialization (right)

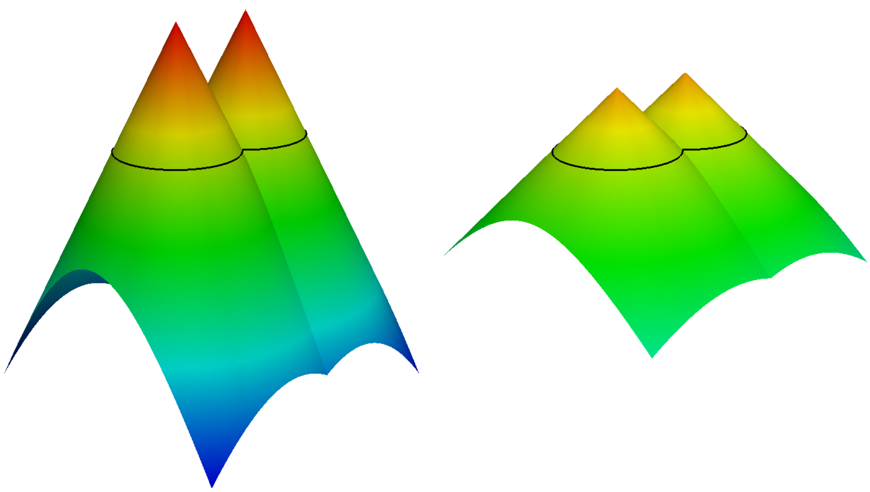

Figure 5. Non-convex overlapping circle interface: initial condition (left) and the level set funciton after reinitialization (right)

5.2. *Rotation of a Slotted Disk*

In this and the following section we solve time-dependent convection problems using the optimal control approach and the convected level set method. Reinitialization techniques based on post-processing are not considered in this numerical study. In our experience they require additional stabilization and tend to produce stronger displacements of the interface if applied at each time step. First, we consider a very challenging non-stationary test case in which the initial data is given as the

h	Initial L^2 proj.		Elliptic reinit.		Elliptic reinit. w. L.P.		OC	
	Error	Order	Error	Order	Error	Order	Error	Order
0.050000	0.008723	1.8378	0.006606	1.3485	0.008727	1.6760	0.174454	4.1036
0.025000	0.002440	2.0102	0.002594	2.0431	0.002731	2.2448	0.010148	1.9720
0.012500	0.000606	1.9306	0.000629	1.9581	0.000576	1.8585	0.002587	1.9562
0.006250	0.000159	2.0128	0.000162	2.0270	0.000159	2.0128	0.000667	1.9942
0.003125	0.000039		0.000040		0.000039		0.000167	

Table II. Convergence test: relative mass (area) error for the non-convex interface.

distance function of a slotted disk, see figure 6. The velocity field is set to

$$\mathbf{v}(t,\mathbf{x}) = \begin{bmatrix} x_2 - \frac{1}{2} \\ \frac{1}{2} - x_1 \end{bmatrix},$$

thus defining a rotation about the center of the domain $\Omega = U_{0.5}(0.5, 0.5)$. In the absence of an inflow boundary portion (the velocity field $\mathbf{v}$ is perpendicular to the outer normal vector) no boundary conditions are required. At $t = 2\pi$, the zero level set of the solution coincides with the initial data so that errors can easily be measured.

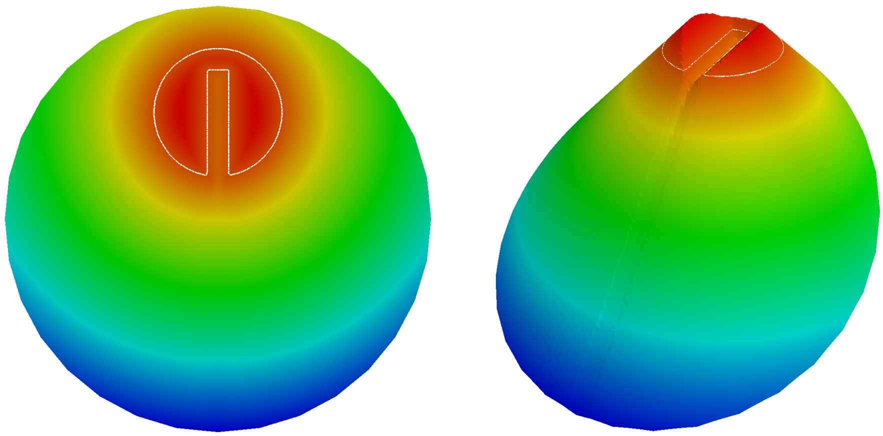

Figure 6. Initial configuration

All numerical computations were carried out using the second-order implicit Crank-Nicolson time stepping scheme and linear finite elements on a mesh with maximal edge length $h_0 = 0.05$ and $\Delta t_0 = \frac{2\pi}{600} \approx 0.01047$ (refinement level $\ell = 0$) and the associated refinements $h_\ell = h_0 \cdot 2^{-\ell}$ and $\Delta t_\ell = \Delta t \cdot 2^{-\ell}$ for $\ell = 1, 2, 3$. We assess the relative averaged mass error by

$$e_{\text{mass}} = \int_0^T \frac{|A(\varphi_h(t)) - A_{\text{exact}})|}{A_{\text{exact}}} \, \mathrm{d}t.$$

In table III the errors for the non-reinitialized standard finite element approach (NR), the Optimal Control approach (OC) and the Convected Reinitialization approach (CR) are listed. Each of the three methods was stabilized by means of SUPG. Throughout all refinement levels, the Eikonal residual of OC is about one half of that for NR, while mass conservation error and L^2 error are of the same order. Note that CR was very sensitive to the choice of its parameter λ and hence may produce better results for more carefully chosen parameters.

As the initial zero interface is not smooth, this is a very challenging test case for reinitialization procedures as they tend to smear discontinuities. OC exhibits similar errors and rates as NR with SUPG stabilization but with a considerably smaller residual of the Eikonal equation. On all refinement levels the same parameter $\beta = 2.5 \cdot 10^{-2}$ was used. Figure 7 shows the zero level sets of the three methods after one full revolution. We observere that both reinitialization methods have problems resolving the sharp corners of the slot. The interface of the OC approach fits the NR interface quite well, i. e. displacements of the interface are rather small.

Non-reinitialized with SUPG stabilization

ℓ	residual Eikonal eq. e_E			L^2 error		rel. mass error e_{mass}	
	Rel. Error	Error	Order	Error	Order	Error	Order
0	3.5493514	0.0201330	0.9054	0.0035952	1.6028	0.0654459	3.2870
1	4.8105934	0.0107488	0.7546	0.0011837	1.1306	0.0067050	1.0431
2	4.1543350	0.0063710	0.8067	0.0005406	1.1789	0.0032538	2.7845
3	4.4149061	0.0036422		0.0002388		0.0004722	

Optimal Control approach ($\beta = 2.510^{-2}$) and SUPG stabilization

ℓ	residual Eikonal eq. e_E			L^2 error		rel. mass error e_{mass}	
	Rel. Error	Error	Order	Error	Order	Error	Order
0	2.1469588	0.0121782	0.8035	0.0046831	1.7306	0.0264582	0.3438
1	3.1227208	0.0069774	0.9333	0.0014111	1.3202	0.0208488	4.8040
2	2.3825698	0.0036539	1.0769	0.0005651	0.8500	0.0007463	1.7621
3	2.0996569	0.0017322		0.0003135		0.0002200	

Convected Reinitialization approach with constant λ and SUPG stabilization

ℓ	residual Eikonal eq. e_E			L^2 error		rel. mass error e_{mass}	
	Rel. Error	Error	Order	Error	Order	Error	Order
0	9.9834836	0.0566294	1.5536	0.0316824	2.1927	0.0776932	1.2649
1	8.6336391	0.0192910	1.3191	0.0069301	1.7719	0.0323301	0.9660
2	5.0415941	0.0077317	1.1186	0.0020293	2.5003	0.0165509	3.1339
3	4.3163510	0.0035609		0.0003587		0.0018854	

Table III. Errors for each method after one full revolution of the slotted disk on different refinement levels

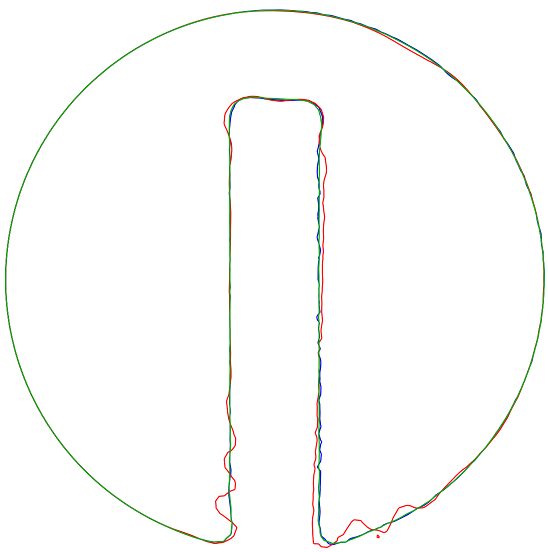

Figure 7. Isocontours of the non-reinitialized approach (green), the Optimal Control approach (blue) and the Convected Reinitialization approach (red)

5.3. *Vortex Deformation of a Circle*

In the previous test cases the zero interface of the solution coincided with the zero interface of the initial data except for rotation and shift. In this case we apply a different velocity field that will significantly deform the zero interface over time. The maximum deformation is reached at half time $t = \frac{T}{2}$, after which the sign is reversed. At final time $t = T$, the initial data is recovered so that we can assess the quality of the interface and the accuracy in terms of mass conservation.

As computational domain we used the unit square with a structured triangular mesh with $h_0 = 0.05$, $\Delta t_0 = 0.01$ and $h_\ell = h_0 \cdot 2^{-\ell}$, $\Delta t_\ell = \Delta t_0 \cdot 2^{-\ell}$ for $\ell = 1, 2, 3$. The velocity field is given by

$$\mathbf{v}(t, \mathbf{x}) = \cos(\tfrac{t\pi}{4}) \left[\begin{array}{c} \sin^2(\pi x_1)\sin(2\pi x_2) \\ -\sin^2(\pi x_2)\sin(2\pi x_1) \end{array} \right]. \tag{35}$$

Note that applying the standard level set method using Crank-Nicolson for time discretization will reproduce the initial data as it is reversible (if no artificial diffusion is introduced by stabilization techniques).
Figure 8 shows the isocontours of the Optimal Control and the Convected Reinitialization approach at time instants $i\frac{t}{4}$, $i = 1, 2, 3, 4$.

ℓ	Non-reinitialized w. SUPG rel. mass error e_{mass}		Convected Reinitialization rel. mass error e_{mass}		Optimal Control rel. mass error e_{mass}	
	Error	Order	Error	Order	Error	Order
0	0.0562404	1.3017	1.0832819	2.0221	0.0278216	1.1142
1	0.0228146	2.7551	0.2667089	3.0191	0.0128519	1.3814
2	0.0033795	2.9307	0.0329006	0.2484	0.0049330	3.1325
3	0.0004432		0.0276965		0.0005625	

Table IV. Mass comparison for Optimal Contral and Convected Reinitialization approaches

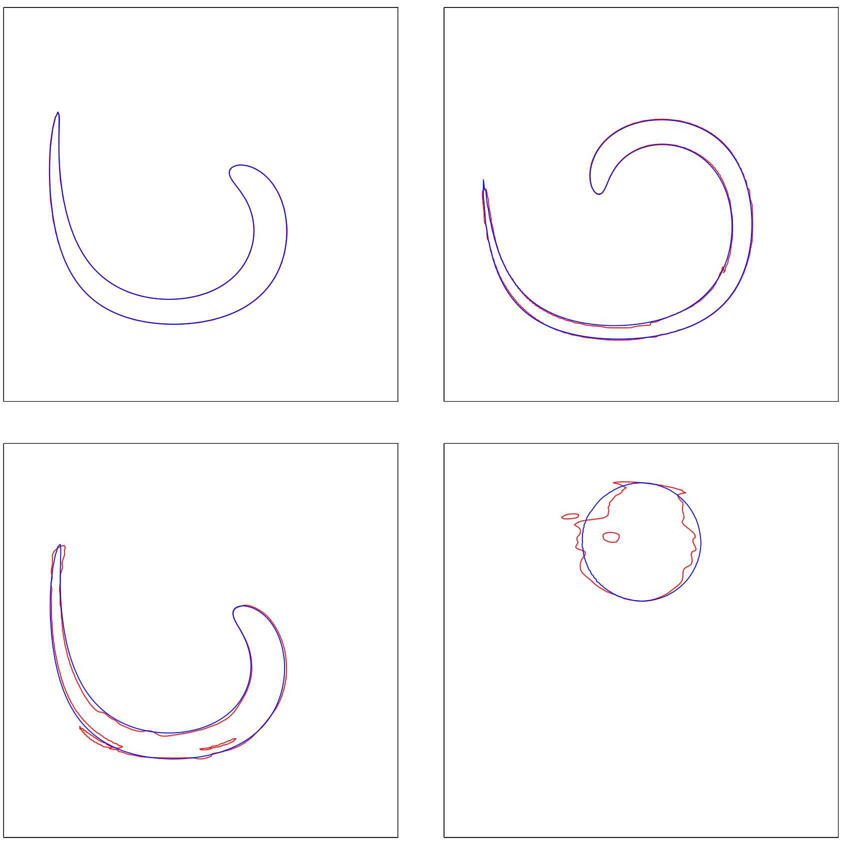

Figure 8. Vortex flow zero level sets for Optimal Control ($\beta = 10^{-1}$) in blue and Convected Reinitialization in red: $t = \frac{T}{4}$ (top left), $t = \frac{T}{2}$ (top right), $t = \frac{3T}{4}$ (bottom left) and $t = T$ (bottom right)

6. SUMMARY

We have presented a new all-at-once strategy to solve the level set transport equation while maintaining the signed distance function property as far as possible. The problem was formulated and the first order optimality conditions were derived and discussed. The benefits of the proposed methodology include the preservation of the zero interface and the possibility of designing a goal-oriented objective functional, for example in the context of shape optimization. Comparison to other PDE-based reinitialization techniques demonstrated the potential of this approach.

REFERENCES

1. Ausas RF, Dari EA, Buscaglia GC. A geometric mass-preserving redistancing scheme for the level set function. *International Journal for Numerical Methods in Fluids* 2011; **65**(8):989–1010, doi:10.1002/fld.2227. URL http://dx.doi.org/10.1002/fld.2227.
2. Sethian J. Fast marching methods. *SIAM Review* 1999; **41**(2):199–235, doi:10.1137/S0036144598347059. URL http://dx.doi.org/10.1137/S0036144598347059.
3. Smolianski A. Numerical modeling of two-fluid interfacial flows. PhD Thesis, University of Jyväskylä 2001.
4. Hysing SR, Turek S. The eikonal equation: numerical efficiency vs. algorithmic complexity on quadrilateral grids 2005; URL http://www.iam.fmph.uniba.sk/amuc/_contributed/algo2005/hysing-turek.pdf.
5. Li C, Xu C, Gui C, Fox M. Distance regularized level set evolution and its application to image segmentation. *Image Processing, IEEE Transactions on* dec 2010; **19**(12):3243 –3254, doi:10.1109/TIP.2010.2069690. URL http://ieeexplore.ieee.org/xpls/abs_all.jsp?arnumber=5557813&tag=1.
6. Parolini N. Computational fluid dynamics for naval engineering problems. PhD Thesis, Lausanne 2004, doi:10.5075/epfl-thesis-3138. URL http://library.epfl.ch/theses/?nr=3138,http://vpaa.epfl.ch/page14334.html.
7. Sussman M, Smereka P, Osher S. A level set approach for computing solutions to incompressible two-phase flow. *Journal of Computational Physics* 1994; **114**:146–159, doi:10.1006/jcph.1994.1155. URL http://dl.acm.org/citation.cfm?id=182718.
8. Tsai YHR, Cheng LT, Osher S, Zhao HK. Fast sweeping algorithms for a class of hamilton-jacobi equations. *SIAM Journal on Numerical Analysis* 2004; **41**(2):pp. 673–694. URL http://www.jstor.org/stable/4101221.
9. Ville L, Silva L, Coupez T. Convected level set method for the numerical simulation of fluid buckling. *International Journal for Numerical Methods in Fluids* 2011; **66**(3):324–344, doi:10.1002/fld.2259. URL http://dx.doi.org/10.1002/fld.2259.
10. Hartmann D, Meinke M, Schröder W. Differential equation based constrained reinitialization for level set methods. *Journal of Computational Physics* 2008; **227**(14):6821 – 6845, doi:http://dx.doi.org/10.1016/j.jcp.2008.03.040. URL http://www.sciencedirect.com/science/article/pii/S0021999108001964.
11. Basting C, Kuzmin D. A minimization-based finite element formulation for interface-preserving level set reinitialization. *Computing* 2013; **95**(1):13–25, doi:10.1007/s00607-012-0259-z. URL http://dx.doi.org/10.1007/s00607-012-0259-z.
12. Cheng LT, Tsai YH. Redistancing by flow of time dependent eikonal equation. *Journal of Computational Physics* 2008; **227**(8):4002 – 4017, doi:http://dx.doi.org/10.1016/j.jcp.2007.12.018. URL http://www.sciencedirect.com/science/article/pii/S002199910700558X.
13. Basting C, Kuzmin D. Optimal control for mass conservative level set methods. *Journal of Computational and Applied Mathematics* 2014; **270**:343 – 352, doi:http://dx.doi.org/10.1016/j.cam.2013.12.040. URL http://www.sciencedirect.com/science/article/pii/S0377042713007139.